Supporting information for

Bicarbonate-controlled reduction of oxygen by the Q_A semiquinone in Photosystem II in membranes

Andrea Fantuzzi[1*], Friederike Allgöwer[2], Holly Baker[1], Gemma McGuire[1], Wee Kii Teh[1], Ana P. Gamiz-Hernandez[2,3], Ville R. I. Kaila[2,3*] and A. William Rutherford[1*]

Content:

Extended methods
Supplementary figures: S1-S16
Supplementary Table S1

Additional information on materials and methods

Materials

5-(Diisopropoxyphosphoryl)-5-methyl-1-pyrroline-N-oxide (DIPPMPO) spin trap was purchased from ENZO and all other chemicals and proteins used were purchased from Sigma (DCMU/diuron, sodium bicarbonate, hydroxylamine, bovine catalase, equine cytochrome *c* (cyt *c*).

Q_A reoxidation using fluorometry

All fluorescence measurements recorded using the Fluorometer FL3000, were carried out with the measuring and actinic flashes set to intensities of 10% and 100% respectively. The single turnover actinic flash duration was set to 50 μs. Each experiment was run for 300 s with the first data point collected 100 μs after the actinic flash.

Stocks of 1 mg Chl/ml PSII and 1M hydroxylamine were prepared in 40 mM of MES and 15 mM of $MgCl_2$ pH 6.5 and stored on ice in the dark until use. For the kinetic measurements the samples were prepared in a septum sealed cuvette. Final concentrations were 60 nM PSII and 250 μM hydroxylamine in 40 mM of MES pH 6.5 and 15 mM of $MgCl_2$. A dark adaptation period was set to 15 minutes, during which the samples were mixed, and oxygen was removed by flushing with argon. Oxygen was re-added to the system with a gas tight syringe by adding oxygenated buffer to the degassed samples in different proportion so that the total volume was maintained constant, avoiding the formation of a headspace in the sealed cuvette. The ratio of oxygenated to degassed buffer was such that the final concentration of oxygen in the sample ranged from 30-230 μM. Final O_2 concentrations, upon each addition, were monitored using the Ocean Optics Neofox Phase oxygen sensor with the Neofox viewer software.

To measure the kinetics of $Q_A^{\bullet-}$ oxidation by O_2, stable $Q_A^{\bullet-}$ was generated to which O_2 could be added in a controlled way. As photochemically generated $Q_A^{\bullet-}$ is normally re-oxidised by either transferring an electron to Q_B or $Q_B^{\bullet-}$, or by back reaction with $S_{2/3}$, these reactions were prevented. We therefore used PSII samples that had sub-stoichiometric amounts of Q_B (1). To estimate the amount of Q_B available for electron transfer, three saturating flashes with a period of 1Hz were sufficient to reduce all the available Q_B and led to the formation of $Q_A^{\bullet-}$ in the majority of the centres (Fig S1). In these conditions $Q_A^{\bullet-}$ re-oxidation occurred with a half-time of about 1 second by recombination with the S_2 or S_3 states. Since S_2-$S_3/Q_A^{\bullet-}$ recombination occurs within seconds, while S_0-$S_1/Q_A^{\bullet-}$ recombination has not been reported and is considered to be stable (2), reduction of the Mn_4O_5Ca cluster back to the S_0/S_1 states should eliminate this competing reaction. It has previously been shown that hydroxylamine is able to act as a reductant to the Mn_4O_5Ca cluster in PSII (3). To avoid over-reduction of the Mn_4O_5Ca cluster, which would lead to loss of the cluster, different hydroxylamine concentrations were tested, and it was found that 250 μM gave good and reproducible results maintaining the cluster intact in the

majority of the centres. Each dark-adapted sample, de-oxygenated by bubbling argon and in the presence of 250 µM of hydroxylamine were subjected to three saturating flashes separated by ~120 s. The fluorescence kinetics were measured upon each saturating flash for 120 s to monitor the accumulation of $Q_A^{\bullet-}$ in a trapped state and assess the proportion of centres in which $Q_A^{\bullet-}$ still decayed by forward electron transfer. The stability of the fluorescence signal, corresponding to the population of trapped $Q_A^{\bullet-}$, was assessed after the third 120 s period, by monitoring the fluorescence without any saturating flash. This allowed sufficient time for any metastable state in the presence of S_2 and S_3, to recombine, leaving a discreet proportion of centres with a long-lived trapped $Q_A^{\bullet-}$. Once a stable fluorescence signal was recorded, oxygenated buffer was added. $Q_A^{\bullet-}$ was stably trapped in approximately 40-50% of the PSII centres.

ROS formation studied under continuous light conditions using cyt c reduction

Samples were prepared in the same way as those used for the single-flash experiment, but hydroxylamine was omitted and samples were illuminated for either 5 or 20 minutes with 50 µmol photons m^{-2} s^{-1} red-filtered light (590 nm long-pass filter), followed by measuring the absorbance spectrum. Cyt *c* concentrations were calculated after subtracting the PSII absorbance spectrum as a background and then subtracting the non-illuminated control. The non-illuminated control and cyt *c* only controls were very similar indicating that there cyt *c* reduction being caused by PSII under dark conditions was negligible.

Additional figures

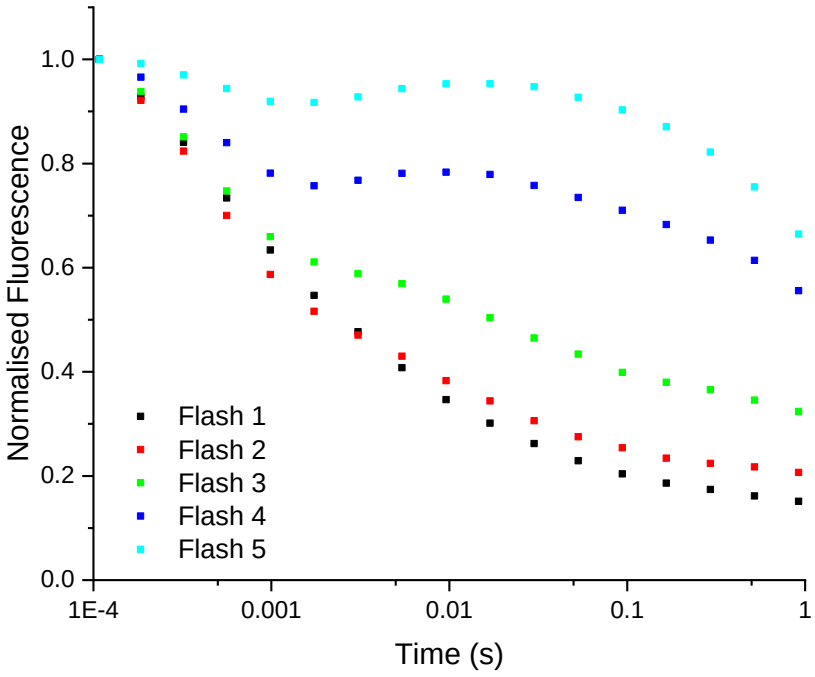

Figure S1. Determination of the amount of available Q_B per reaction center. Fluorescence kinetics decays were measured for PSII membrane fragments (60 nM PSII) in a 40 mM MES buffer, 5 mM $MgCl_2$, pH 6.5, upon each actinic flash in a series of flashes with a 1 Hz frequency. Kinetics after the first and the second flash clearly show a decay with a half-life in the milliseconds, characteristic of forward electron transfer from $Q_A^{\bullet-}$ to both Q_B and $Q_B^{\bullet-}$. On the third and fourth flashes the amplitude of this milliseconds kinetic decay was progressively reduced to 40% and 25%, respectively, with the rest showing much slower decay times. On the fifth flash, the main decay half-life was approximately one second, typical of the $S_2Q_A^{\bullet-}$ recombination. These data show that a maximum of two quinones are available per reaction center.

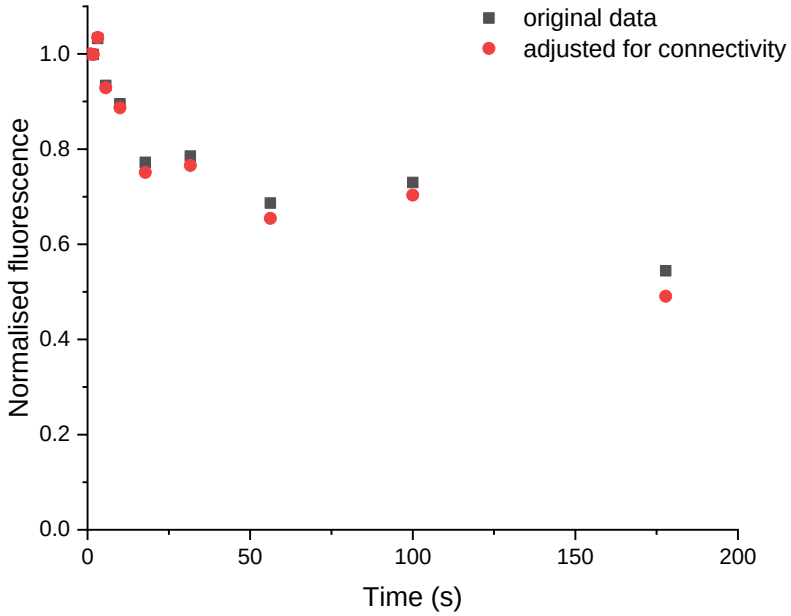

Figure S2. The effect of antenna connectivity on the fluorescence-based measurement of the kinetics of $Q_A^{\bullet-}$ re-oxidation by O_2. Fraction of $Q_A^{\bullet-}$ obtained from the fluorescence kinetics data (grey squares symbols) obtained for a degassed sample of PSII membrane fragments (60 nM PSII) in the presence of 250 µM hydroxylamine in a 40 mM MES buffer, 5 mM $MgCl_2$, pH 6.5, when 40 µM of oxygen was added. These data points are compared with the fraction of $Q_A^{\bullet-}$ obtained by correcting the fluorescence values for the effect of connectivity between the reaction centres. Due to antenna connectivity the exciton visiting a closed centre has a significant probability of continuing its random walk and eventually hitting an open trap (5, 6). A consequence is that the fluorescence yield *F* depends on the fraction of closed centres, *c*, in a hyperbolic rather than linear way, according to the equation:

$$F(c) = c/(1+J-Jc) \qquad \text{(SE1)}$$

The parameter *J* expresses the antenna connectivity. The non-linear relationship between the fluorescent yield *F* and the concentration of reduced Q_A has consequences on the correct determination of the fraction of reduced Q_A as a function of time in the decay. This effect was corrected using the *J* factor previously determined of 1.6.

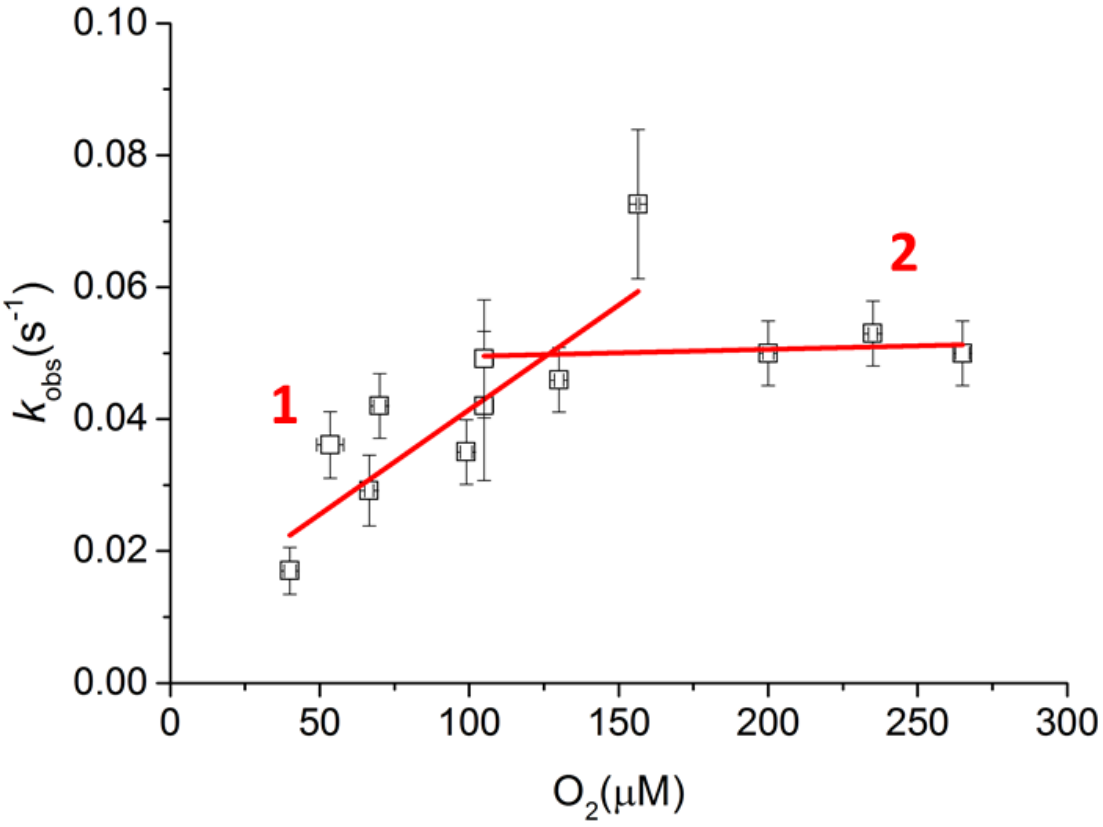

Figure S3. Kinetics of $Q_A^{\bullet-}$ oxidation. Rate of $Q_A^{\bullet-}$ oxidation plotted as a function of O_2 concentration. Data from figure 2C in the main paper fitted with two linear behaviours corresponding to the second (1) and zero (2) order of the reaction. The slope of the linear fitting (1) yields the second order rate constant for the bimolecular interaction between $Q_A^{\bullet-}$ and O_2.

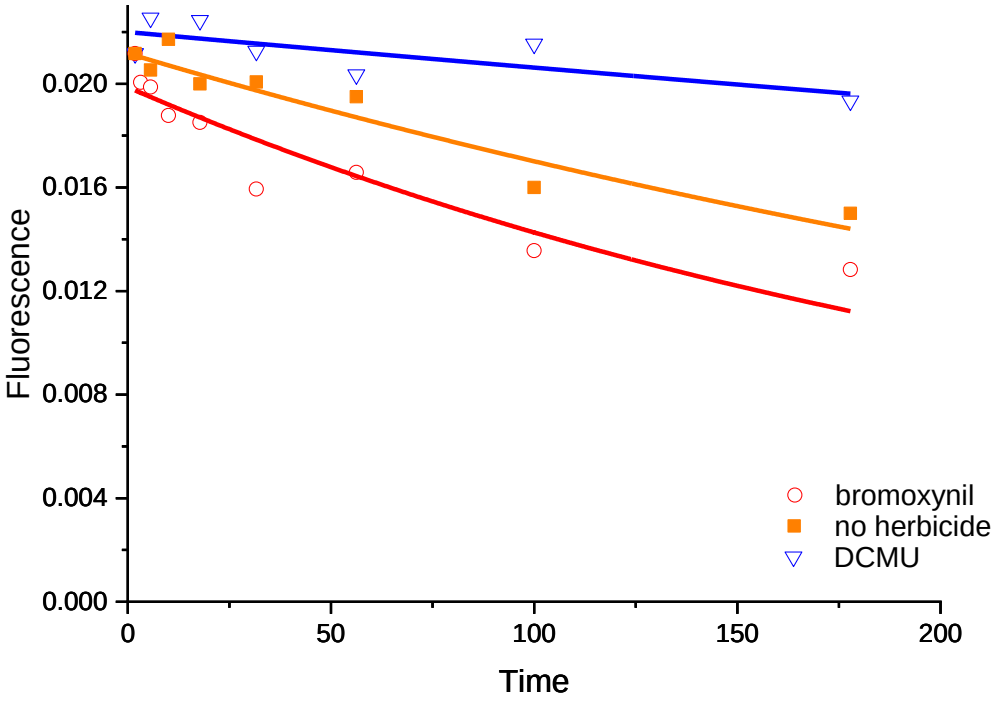

Fig S4. Fluorescence decay from trapped $Q_A^{\bullet-}$ in the absence of oxygen. The slow decay was assigned to the $Tyr_D^{\bullet}$ $Q_A^{\bullet-}$ recombination. The decays are shown in the absence and the presence of added herbicides. The measured kinetics in the presence of bromoxynil (red circles and line) is faster than the one in the presence of DCMU (blue triangles and line). The kinetic measured in the absence of the herbicides (orange squares and line) shows rates in between the other two kinetics.

These data, therefore, confirm firstly that the slow fluorescence decay observed in the trapped $Q_A^{\bullet-}$ in the absence of oxygen is due to the recombination of $Q_A^{\bullet-}$ with a relatively stable electron acceptor thought to be $Tyr_D^{\bullet}$ (4). Secondly, that bromoxynil is bound to the Q_B site also in the presence of hydroxylamine and behaves as expected in the untreated PSII.

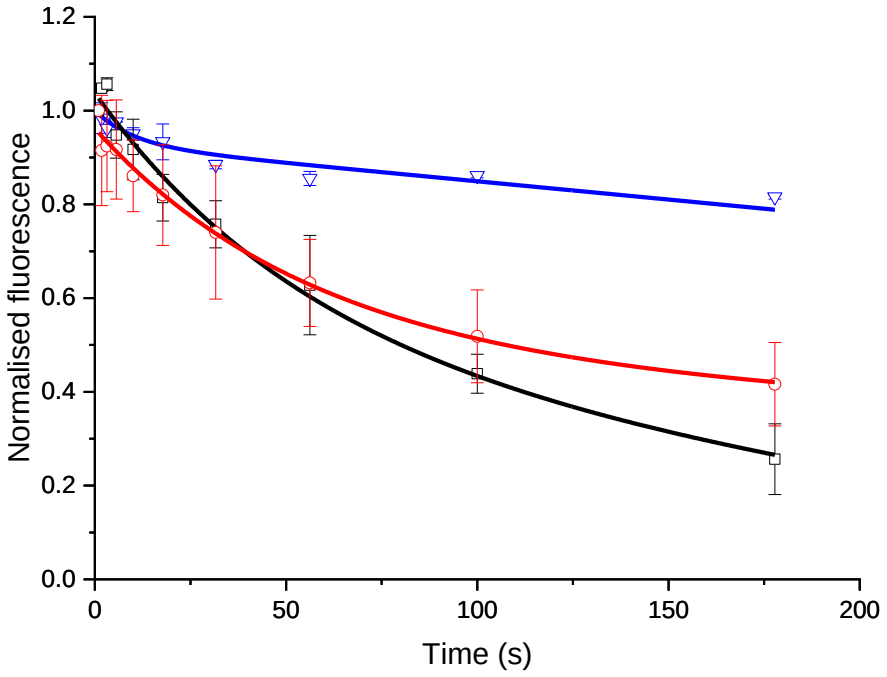

Figure S5. The effect of Q_B-site herbicides on the kinetics of $Q_A^{\bullet-}$ re-oxidation by O_2. Fraction of $Q_A^{\bullet-}$ obtained after three saturating flashes of a degassed sample of PSII membrane fragments (60 nM PSII cores) in the presence of 250 µM hydroxylamine in a 40 mM MES buffer, 5 mM $MgCl_2$, pH 6.5. All the data are fitted to equation 1. Effect of the addition of Q_B site inhibitors. Control experiment with oxygen and no herbicide is shown for comparison (open black symbols). 10 µM DCMU (open blue symbols) or 100 µM bromoxynil (open red symbols) were added prior to the degassing step and the kinetics were measured upon addition of 40±3 µM O_2.

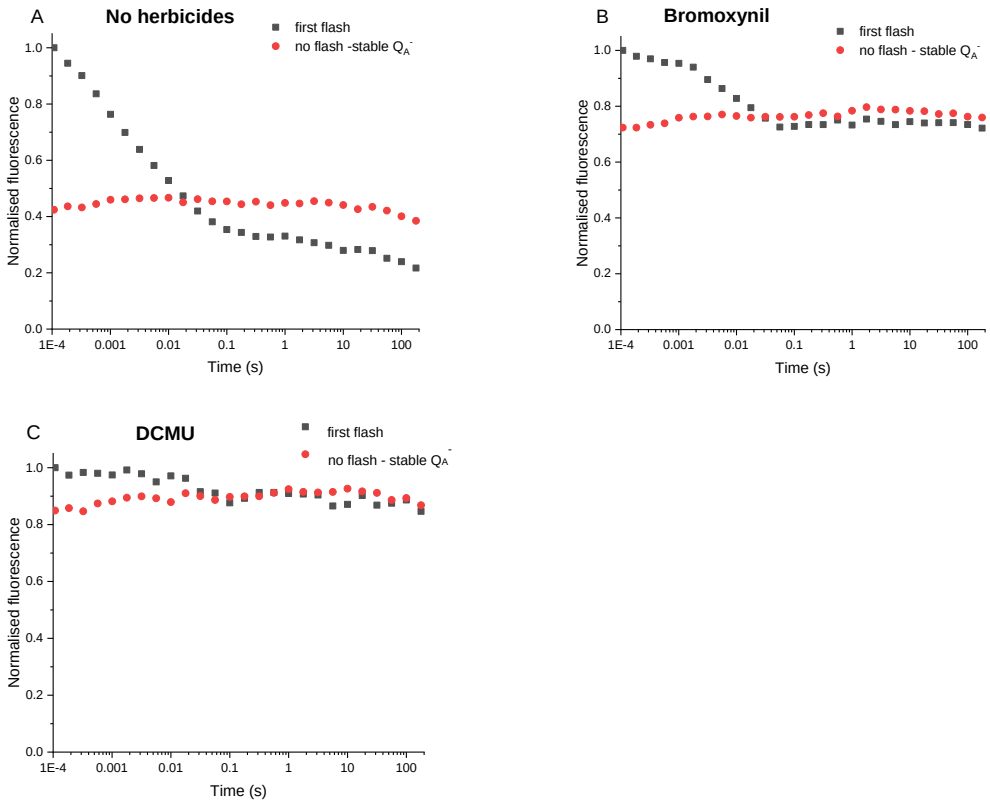

Fig S6. $Q_A^{\bullet-}$ reoxidation kinetics in the presence of 250 µM hydroxylamine and no oxygen. Fluorescence decay kinetics recorded upon the first of the three saturating flashes are shown as black squares. In the absence of herbicides (**A**), on the first flash the largest proportion of the decay is dominated by forward electron transfer from $Q_A^{\bullet-}$ to either Q_B or $Q_B^{\bullet-}$ (~1 ms). Approximately 30% of the centers show $Q_A^{\bullet-}$ in a locked state (due to the depleted PQ pool, the absence of O_2, and "irreversible" donation from, e.g., NH_2OH, S_0, Tyr_D, or $Cytb_{559}$). This percentage was found to increase in the subsequent flashes to a level of 40-50% (see fluorescence level of the red data points in panel **A**). In the presence of both bromoxynil and DCMU, the fluorescence profile following the first flash is instead dominated by $Q_A^{\bullet-}$ in the locked state (panels **B, C**). DCMU shows 10% of the centers doing $S_2Q_A^{\bullet-}$ charge recombination (a few seconds), while Bromoxynil shows about 10% of centers doing forward electron transfer from $Q_A^{\bullet-}$ to Q_B/ $Q_B^{\bullet-}$ (i.e., centers where bromoxynil does not bind) and about 15% of centers that appears to be doing $S_2Q_A^{\bullet-}$ charge recombination (~500 ms in competition with reduction of S_2 by NH_2OH). The 10% of centers doing forward electron transfer in the presence of bromoxynil is due to the herbicide lower binding affinity. Nevertheless, the data clearly show that bromoxynil binds to the majority of centers even when hydroxylamine is present. Importantly, in all the experimental conditions used for the observations made here, we only studied the majority fraction of centers in which $Q_A^{\bullet-}$ was stably trapped. Any centers in which $Q_A^{\bullet-}$ undergoes charge recombination will be absent from the measurement because of the addition of oxygen was performed only after the signal of the stable $Q_A^{\bullet-}$ was recorded without any additional saturating light pulses (red data points in the figure).

A

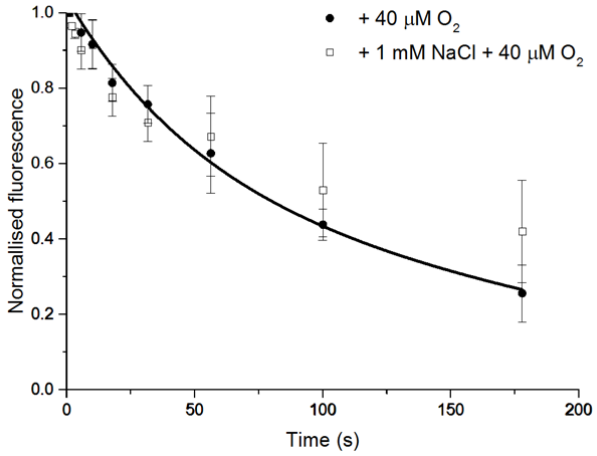

B

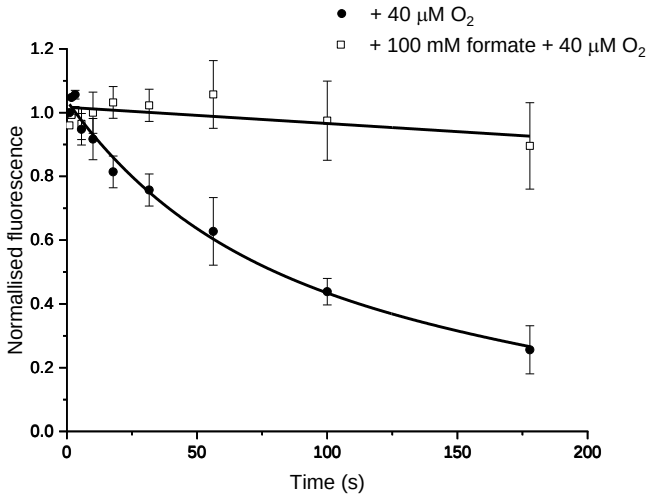

Figure S7. Kinetics of $Q_A^{\bullet-}$ re-oxidation by O_2: effect of NaCl (control for bicarbonate addition) and effect of formate. Fraction of $Q_A^{\bullet-}$ obtained after three saturating flashes of a degassed sample of PSII membrane fragments (60 nM PSII) in the presence of 250 μM hydroxylamine in a 40 mM MES buffer, 5 mM $MgCl_2$, pH 6.5. 40 μM of O_2 was added in the absence or in the presence of (**A**) 1mM NaCl and (**B**) 100 mM formate.

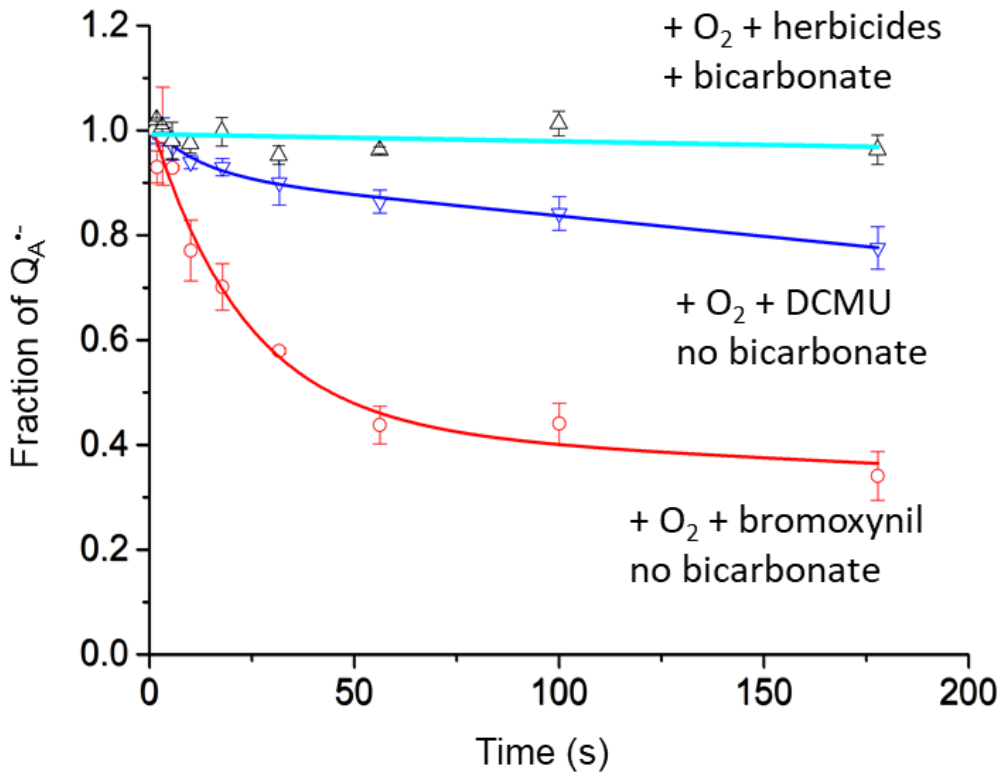

Figure S8. Kinetics of $Q_A^{\bullet-}$ oxidation. (A) Effect of presence of bicarbonate of the influence of herbicides on the kinetics of $Q_A^{\bullet-}$ re-oxidation by O_2. Data from figure 2B (blue and red curves for sample with 10 µM DCMU and 100 µM bromoxynil respectively) are compared with the combined effect of either of two herbicides (DCMU or bromoxynil) and 1 mM bicarbonate (cyan curve). For clarity only the data with DCMU + bicarbonate are shown as those with bromoxynil + bicarbonate are almost identical.

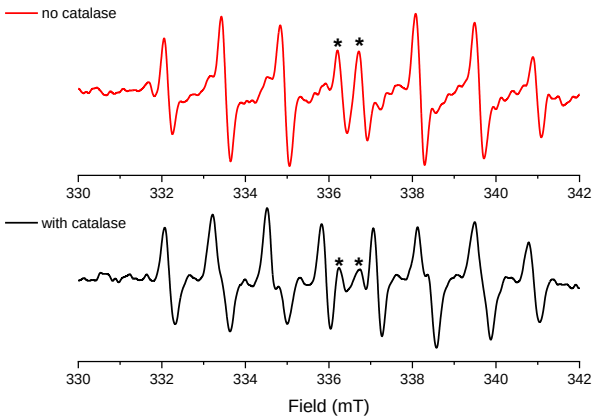

Fig S9 Characterisation of the EPR spectra of the DIPPMPO spin probe adducts. In our initial measurements aimed at identifying the product of the reduction of oxygen by $Q_A^{\bullet-}$ sing the DIPPMPO EPR spin probe, we observed a spectrum (red trace) with features reminiscent of the DIPPMPO-OH adduct (7). DIPPMPO-OH, formed by the reaction of DIPPMPO with hydroxyl radical, has specific features, labelled with asterisks (*) in the figure, that are unique when compared with the EPR spectrum of the DIMPPO-OOH obtained from the reaction with superoxide (see Ref 7 for a comparison of the spectra). Addition of catalase, which removes peroxide (formed by dismutation of the $O_2^{\bullet-}$), which could give rise to $OH^{\bullet}$ by Fenton chemistry, resulted in a spectrum (black trace) in which the contribution of the DIPPMPO-OH adduct was greatly reduced based on the intensity of the two central peaks (*).

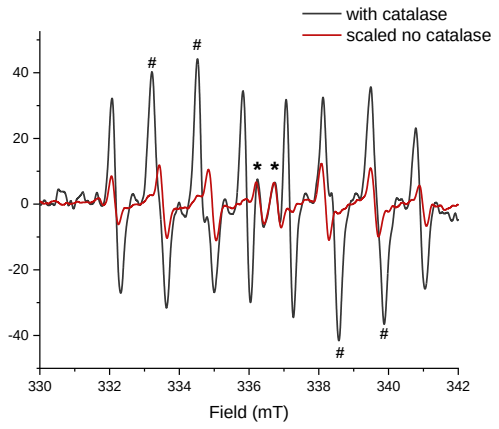

Fig S10 To quantify the residual contribution of the DIPPMPO-OH adduct upon addition of catalase, we scaled the spectrum obtained without catalase, to match the intensity of the two centra peaks (*). Based on this scaling we assessed that about 20% of DIPPMPO-OH is still present when catalase is added. Nevertheless, the scaling also show that the peaks used for the identification of DIPPMPO-OOH (#) have minimal contribution from the DIPPMPO-OH spectra.

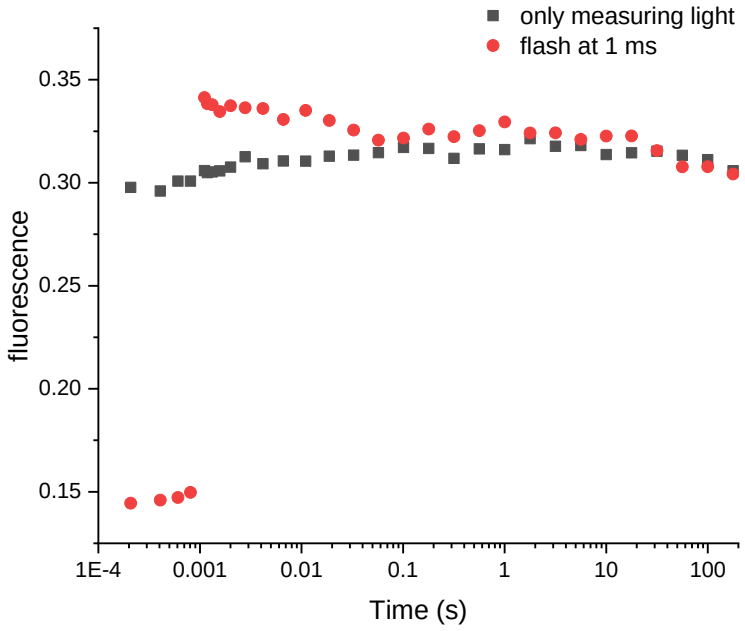

Figure S11. Assessing the actinic nature of the measuring light in the fluorescence experiments. Fluorescence was measured for a degassed sample of PSII membrane fragments (60 nM PSII) in the presence of 250 µM hydroxylamine in a 40 mM MES buffer, 5 mM $MgCl_2$, pH 6.5 and 10 µM DCMU. Each data point in the graph represents a fluorescence value detected by a single weak measuring pulse from a 650nm LED. The red filled circles represent the measurements obtained when a single saturating flash was given at 1 ms to a sample that had been dark-adapted for 15 minutes during the degassing process. The fluorescence level remains high and constant after the flash with only a small decay in the hundreds of seconds. The black filled squares represent the fluorescence measurement done on the same sample immediately after recording the first kinetic data set. As a result, the first data point (black points) coincides with the last data point of the previous kinetics data set (red points). The fluorescence values remain high and relatively stable, showing the same slow decay in the hundreds of seconds. This slow decay corresponds to the linear decay shown by the orange points in figure 2A. Nevertheless, a small rise in fluorescence can be observed when the frequency of the weak measuring flashes is high, between 1 and 10 ms. When instead the frequency is low in the rest of the kinetics the fluorescence values remain constant. These data show that the measuring flashes are slightly actinic when their frequency is high, between 1 and 10 ms, leading to a small accumulation, approximately 10%, of reduced Q_A.

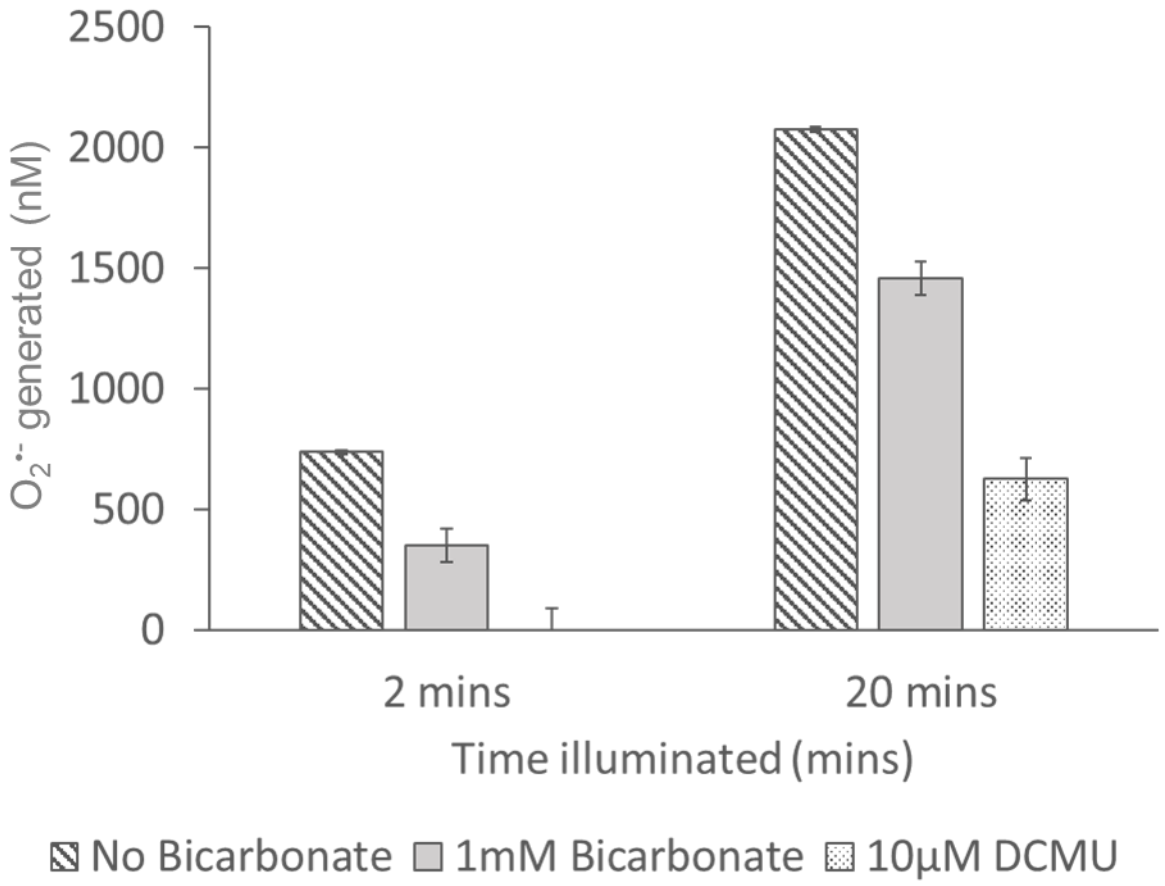

Figure S12. $O_2^{\bullet-}$ quantified as reduced cytochrome *c* in the absence (striped) and in the presence of either 1 mM bicarbonate (grey) or 10 mM DCMU (dots). Sample was illuminated for either 2 or 20 minutes with 50 µmol photons m^{-2} s^{-1} red light (590 nm long-pass filter). PSII membrane fragments (60 nM PSII) in 40 mM MES buffer, 5 mM $MgCl_2$, pH 6.5.

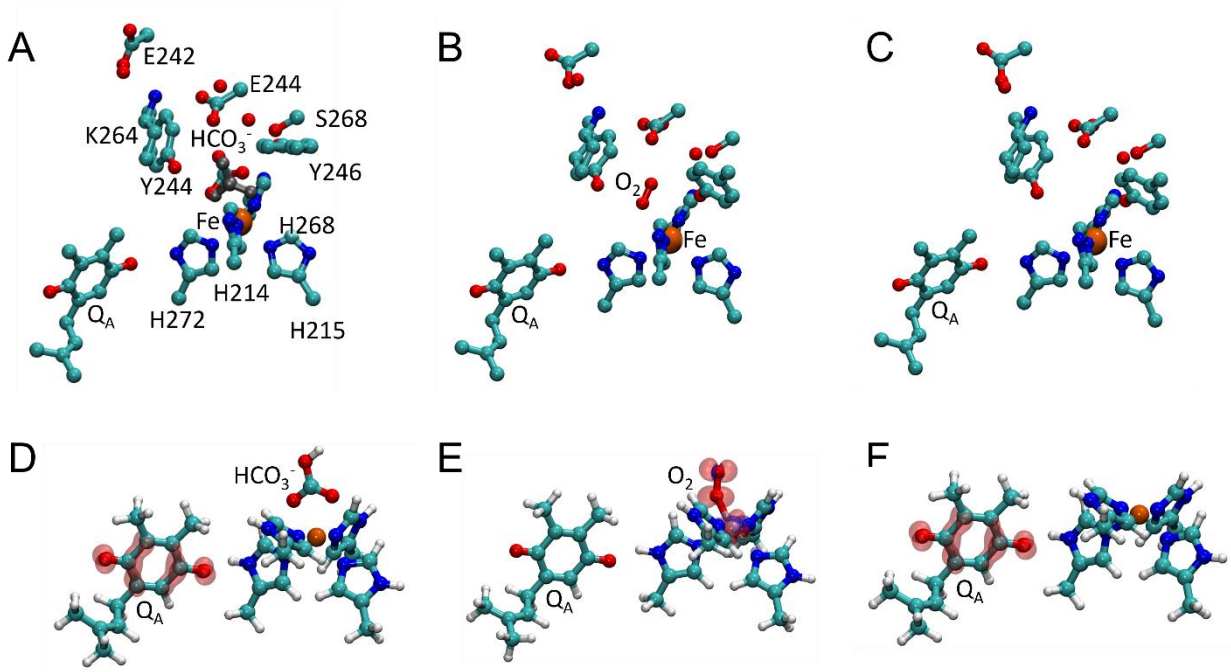

Figure S13. DFT models and QM/MM systems. The QM region comprises the non-heme Fe^{2+} complex with its four coordinating histidine residues ($His215^{D1}$, $His272^{D1}$, $His214^{D2}$, and $His268^{D2}$), the plastoquinone Q_A, $Glu244^{D1}$, $Tyr246^{D1}$, $Ser268^{D1}$, $Tyr244^{D2}$, $Lys264^{D2}$, in addition to three crystal water molecules and **(A)** the HCO_3^--bound state (Fe^{3+}-HCO_3^- shown in grey); **(B)** the O_2-bound state, and **(C)** the state lacking the exchangeable HCO_3^- ligand. (**D**)–(**F**) spin density differences (red/blue sphere ±0.001e for alpha/beta spin) after adding an electron into models A-C: (**D**) the HCO_3^--bound state, (**E**) the O_2-bound state, and (**F**) the state lacking exchangeable ligands. For clarity, panels D-F show only Q_A, the iron and its ligands (*i.e.*, the four histidines in addition to either HCO_3^- or O_2).

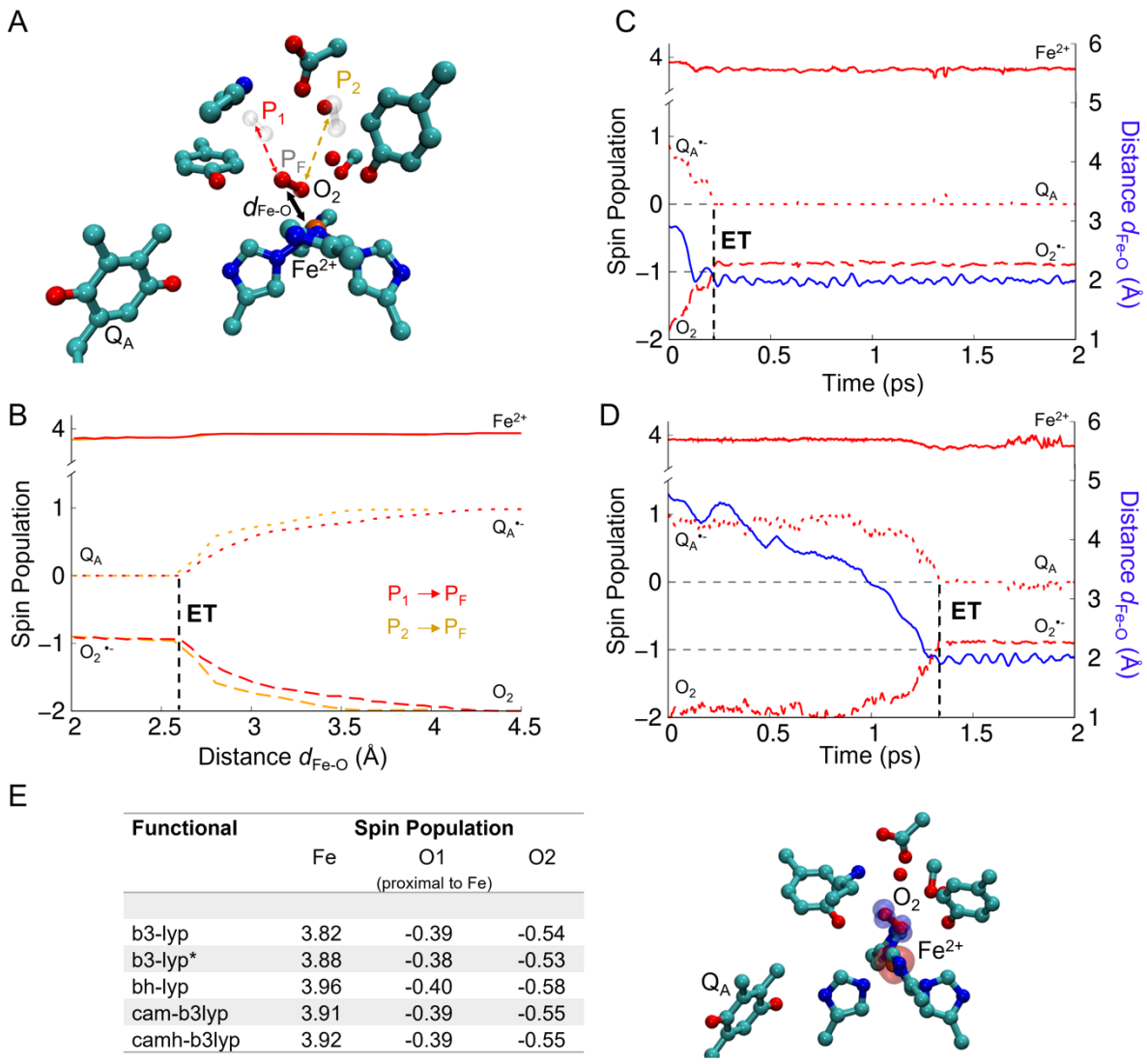

E

Functional	Spin Population		
	Fe	O1 (proximal to Fe)	O2
b3-lyp	3.82	-0.39	-0.54
b3-lyp*	3.88	-0.38	-0.53
bh-lyp	3.96	-0.40	-0.58
cam-b3lyp	3.91	-0.39	-0.55
camh-b3lyp	3.92	-0.39	-0.55

Figure S14. Electron transfer dynamics at the non-heme iron center. (A) To probe at which Fe-O_2 distance the electron transfer (ET) is triggered, the O_2 was placed at two different starting positions (P_1 and P_2) and then gradually moved closer towards the Fe^{2+} (final geometry optimized position: P_F). **(B)** spin populations change with respect to the $d_{Fe\text{-}O}$ distance. The electron transfer is completed at a Fe-O_2 distance of around 2.6 Å (ET; black dashed line) independent of the starting position. **(C)** and **(D)** ET-dynamics during QM/MM MD simulations. The simulations were initiated from different initial Fe-O_2 distances, **(C)** 2.9 Å and **(D)** 4.8 Å. In both simulations, the electron transfer initiates at ~3 Å and is complete at ~2 Å (ET; black dashed line). Spin population on Q_A are shown as dotted lines; on Fe^{2+} as solid lines, and on O_2 as dashed lines. (**E**) Spin population analysis (table) using different density functionals and the spin density (right figure) show that the electron transfer from $Q_A^{\bullet-}$ to Fe-O_2 is supported using different density functionals.

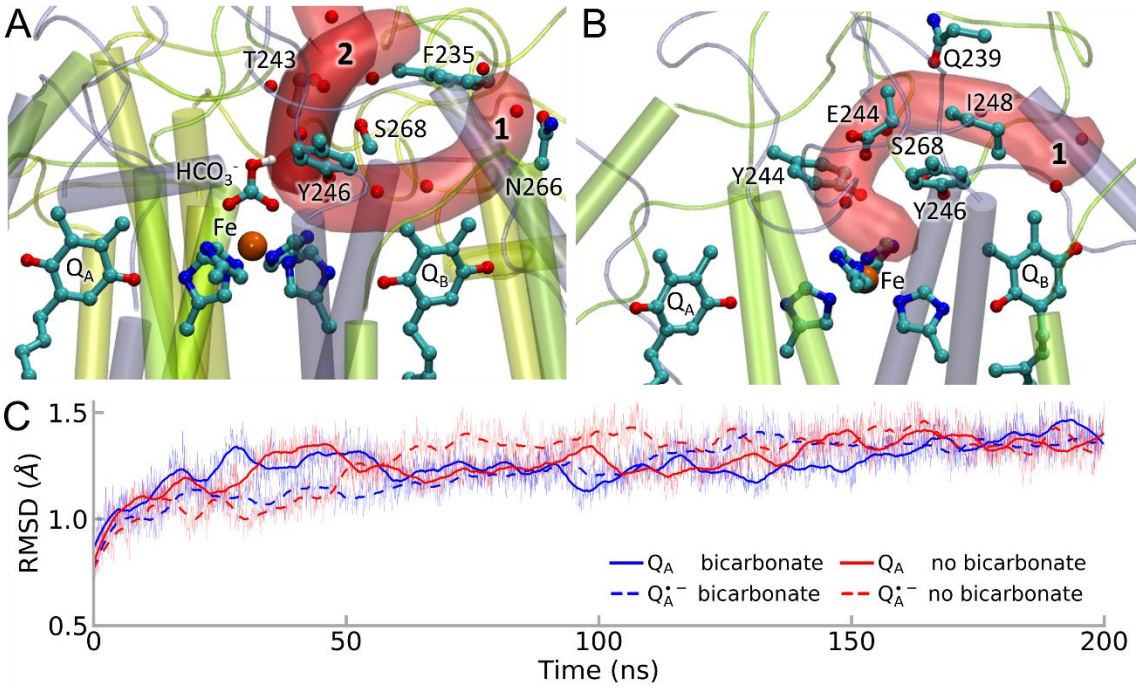

Figure S15. Water-filled tunnels forming around the plastoquinone site during MD simulations of PSII. (**A**) In the HCO_3^--bound form, tunnels 1 and 2 are present near the non-heme iron site, but water molecules are blocked from reaching the non-heme iron center by i) the bicarbonate itself (shown here) and ii) the nearby Lys264, which undergoes conformational changes relative to the crystal structure and leads to a decrease of hydration (shown in Fig. 4F). (**B**) When no exchangeable ligands were bound to the Fe^{2+}, the tunnels extended to the Fe^{2+}, allowing water or dioxygen to access the non-heme iron site. (**C**) Root-mean-square-deviations (RMSD) of the complete PSII during MD simulations, showing stabilization during the initial 100 ns.

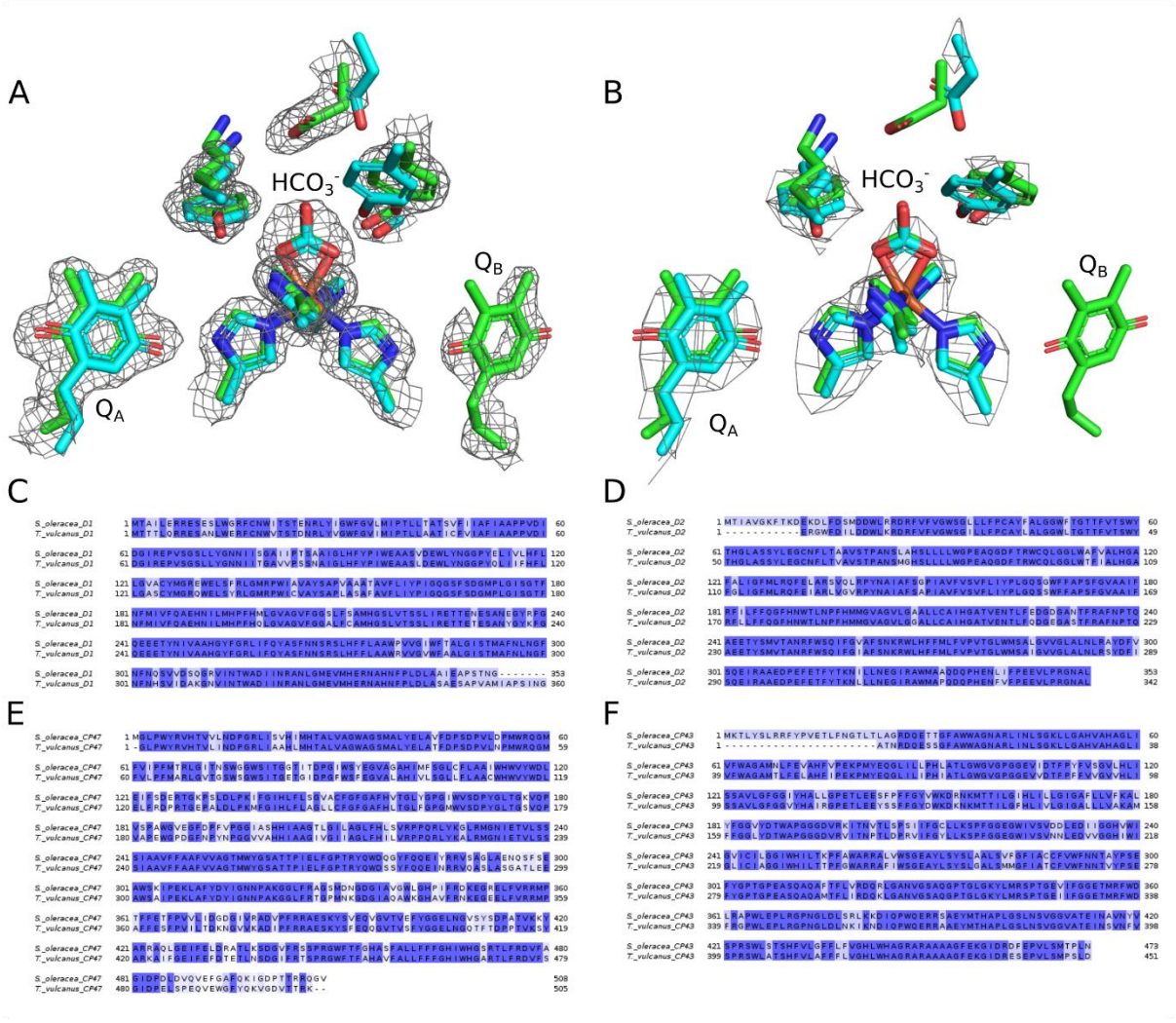

Fig S16. Structural comparison between A) the cyanobacterial (*T. vulcanus*, PDB ID: 3WU2, in red). Density is shown at 1σ level. B) Spinach PSII (*S. oleracia*, PDB ID: 3JCU, in blue), with cryoEM densities (EMD-6617) at shown 4.5σ level. The Q_B is unresolved but modeled based on the cyanobacterial structure. C-D) Sequence comparison between PSII from *T. vulcanus* and *S. oleracia* for subunits A) D1, B) CP47, C) CP43 and D) D2. Identical residues are marked in dark blue; similar residues in light blue; and different residues in white. The overall sequence identity is 85% for D1, 76% for CP47; 80% for CP43; and 87% for D2.

Table S1. Summary of DFT, QM/MM-MD, and classical MD simulations. Simulations 11 and 12 were initiated with initial $Fe^{2+}\cdots O_2$ distances, of 2.9 Å and 4.8 Å respectively.

Simulation	Fe^{2+}-ligand	Redox State of Q_A	Method	System size (Atoms)	Simulation length
1	-	Q_A	DFT	155	*optimization*
2	-	$Q_A^{\bullet-}$	DFT	155	*optimization*
3	HCO_3^-	Q_A	DFT	160	*optimization*
4	HCO_3^-	$Q_A^{\bullet-}$	DFT	160	*optimization*
5	O_2	Q_A	DFT	157	*optimization*
6	O_2	$Q_A^{\bullet-}$	DFT	157	*optimization*
7	H_2O	Q_A	DFT	158	*optimization*
8	H_2O	$Q_A^{\bullet-}$	DFT	158	*optimization*
9	-	$Q_A^{\bullet-}$	QM/MM MD	65,197	2 ps
10	HCO_3^-	$Q_A^{\bullet-}$	QM/MM MD	65,203	2 ps
11	O_2	$Q_A^{\bullet-}$	QM/MM MD	65,202	2 ps
12	O_2	$Q_A^{\bullet-}$	QM/MM MD	65,202	2 ps
13	-	Q_A	MD	425,395	200 ns
14	-	$Q_A^{\bullet-}$	MD	425,396	200 ns
15	HCO_3^-	Q_A	MD	425,401	200 ns
16	HCO_3^-	$Q_A^{\bullet-}$	MD	425,400	200 ns

SI References

1. A. Krieger-Liszkay, A. W. Rutherford, Influence of Herbicide Binding on the Redox Potential of the Quinone Acceptor in Photosystem II: Relevance to Photodamage and Phytotoxicity. *Biochemistry* **37**, 17339-17344 (1998).
2. A. W. Rutherford, A. R. Crofts, Y. Inoue, Thermoluminescence as a probe of Photosystem II photochemistry. The origin of the flash-induced glow peaks. *Biochim. Biophys. Acta - Bioenergetics* **682**, 457-465 (1982).
3. R. D. Guiles *et al.*, The S0 state of photosystem II induced by hydroxylamine: differences between the structure of the manganese complex in the S0 and S1 states determined by x-ray absorption spectroscopy. *Biochemistry* **29**, 486-496 (1990).
4. G. N. Johnson, A. Boussac, A. W. Rutherford, The origin of 40–50°C thermoluminescence bands in Photosystem II. *Biochim. Biophys. Acta - Bioenergetics* **1184**, 85-92 (1994).
5. A. Joliot, P. Joliot, Etude cinétique de la réaction photochimique libérant l'oxygène au cours de la photosynthèse. *C.R. Acad. Sci. Paris* **258**, 4622-4625 (1964).
6. J. Lavergne, H. W. Trissl, Theory of fluorescence induction in photosystem II: derivation of analytical expressions in a model including exciton-radical-pair equilibrium and restricted energy transfer between photosynthetic units. *Biophys. J.* **68**, 2474-2492 (1995).
7. S. Sheinok, P. Leveque, P. Sonveaux, B, Driesschaert, B. Gallez, Comparison of different methods for measuring the superoxide radical by EPR spectroscopy in buffer, cell lysates and cells. Free Rad. Res. 52, 1182-1196 (2018).